Title

Ion-momentum imaging of dissociative attachment of electrons to molecules

Journal

Journal of Physics B Atomic Molecular and Optical Physics, 49(22)

ISSN

0953-4075

Authors

Slaughter, DS

Belkacem, A

McCurdy, CW

et al.

Publication Date

2016-11-28

DOI

10.1088/0953-4075/49/22/222001

Peer reviewed

TOPICAL REVIEW

Ion-momentum imaging of dissociative attachment of electrons to molecules

D. S. Slaughter[1] A. Belkacem[1] C. W. McCurdy[1,2] T. N Rescigno[1] and D. J. Haxton[1]

[1]Lawrence Berkeley National Laboratory, Chemical Sciences, Berkeley, CA 94720

[2]Department of Chemistry, University of California, Davis, CA 95616

E-mail: dsslaughter@lbl.gov, danhax@gmail.com, cwmccurdy@lbl.gov, tnrescigno@lbl.gov, abelkacem@lbl.gov

Abstract. We present an overview of experiments and theory relevant to dissociative electron attachment studied by momentum imaging. We describe several key examples of characteristic transient anion dynamics in the form of small polyatomic electron-molecule systems. In each of these examples the so-called axial recoil approximation is found to break down due to correlation of the electronic and nuclear degrees of freedom of the transient anion. Guided by anion fragment momentum measurements and predictions of the electron scattering attachment probability in the molecular frame, we demonstrate that accurate predictions of the dissociation dynamics can be achieved without a detailed investigation of the surface topology of the relevant electronic states or the fragment trajectories on those surfaces.

Contents

1. Introduction

The fixed-nuclei electron-molecule scattering problem gives a valuable, but often incomplete, description of the physics of the full collision. This is especially true in the case of resonant collisions where the incoming electron can be temporarily trapped in a transient negative ion state, which in turn can change the electronic environment that binds the target nuclei. Indeed, resonant collisions between low-energy electrons and molecules can provide an efficient mechanism for channeling electronic energy into nuclear degrees of freedom through processes such as vibrational excitation or dissociative electron attachment (DEA). The nuclear dynamics problem, i.e. the set of processes that control the flow of energy into nuclear degrees of freedom, is of fundamental importance in studying electron collisions with polyatomic targets and is key to developing an understanding of electron-driven chemistries in a variety of contexts, from modeling energy flow in low-temperature plasma processing gases[1] to the study of gas excimer lasers and planetary atmospheres, to secondary electron - driven chemistry on surfaces[2, 3]. In the case of DEA, the resurgence of interest, on both the experimental and theoretical fronts, that has taken place over the past decade and a half has been triggered by the importance of DEA in understanding radiation induced damage in biological cells and the fact that DEA leads to site selective bond-breaking and can be responsible for double-strand breaks in DNA[4, 5].

DEA was extensively studied in the the 1970s and early 1980s[6, 7, 8]. Most of the experiments that were reported measured total cross sections for fragment anions as a function of incident electron energy. Notable exceptions were the kinetic energy- and angle-resolved experiments of Van Brunt and Kieffer[9, 10] and Hall *et al.*[11, 12], who pioneered the experimental approaches to measure crucial dynamical information of dissociating anions. Early theoretical studies of DEA were based on semi-empirical models derived from the formal resonance theory developed in the 1960s[13, 14, 15]. Characteristic of these studies was the fact that while the resonance formalism became increasingly detailed, with elaborate resonance models of increasing complexity involving non-local, complex interaction potentials, the dynamical treatment of the nuclei was invariably one-dimensional, involving a single dissociative coordinate. The theory was thus restricted to diatomics or to polyatomic targets with a presumed single dissociative degree of freedom.

With a new generation of ion detection schemes featuring COLTRIMS (COLd target recoil ion momentum spectroscopy)-like reaction microscopes[16, 17, 18, 19] or velocity-slice imaging spectrometers[20, 21, 22], 4π detection of fragment ions is possible. The emphasis in current DEA experiments with such detectors has shifted from the measurement of total cross sections to analysis of the fragment ion angular distributions from polyatomic targets of increasing complexity. How can we extract knowledge of multidimensional dissociation dynamics from such experiments? A question to ponder in a typical DEA reaction

$$\begin{aligned} e^- + M \rightarrow (M^-)^* &\rightarrow A^- + B \\ &\rightarrow A + B^- \end{aligned} \tag{1}$$

is the following: while there are generally several negative ion resonances in electron scattering with a typical molecule, there is is generally only one bound anion state of an atomic or molecular fragment. So how can more than one of those resonances produce the same anion product? Or one resonance produce two different anion arrangements? These questions have resulted in a number of combined theoretical/experimental

studies of polyatomic DEA which have revealed some unexpected mechanisms. A recurring theme that has emerged from these DEA studies is that, even for small polyatomic targets, the process can be governed by complex electronic and nuclear dynamics. This dynamics can be intrinsically polyatomic, i.e. multi-dimensional, in character, involving symmetry-breaking deformations and conical intersections. The combination of *ab initio* theory and experimental measurements using modern imaging techniques is the key to unraveling this dynamics. How that symbiosis of theory and experiment has evolved over the past decade is the subject of this topical review.

In this work, we do not attempt to perform a comprehensive review the state of dissociative electron attachment experiments or theory and instead refer the reader to the excellent reviews in Refs [6, 7, 8, 23, 24, 25, 26, 27, 28]. Instead we focus on some of the recent developments in momentum imaging that have brought new perspective to our understanding of DEA dynamics and revealed important features that we illustrate in selected examples.

2. Experimental techniques

Recent advances in electron sources have recently lead to ultrafast time-resolved electron scattering experiments[29, 30], however direct time-resolved studies of a transient metastable anion formed by electron attachment remain experimentally intractable due the very short timescales of single molecule dissociation that demand even higher time resolution. Considerable technical challenges remain that must be overcome to produce and transport low energy electrons with a pulse duration less than $\sim$100 fs[29, 30, 31, 32]. On the other hand, the experimental approaches that interrogate the final states following DEA can lend much insight into these dynamics. Differential measurements of the kinetic energy or angular distributions of the DEA products are exquisitely sensitive to the dynamics of the transient anion and have shown great success in guiding highly sophisticated *ab initio* theoretical treatments that accurately describe electronic and nuclear motion beyond the Born-Oppenheimer Approximation. Most experimental studies of DEA to date have explored the signatures of the dissociating anion that are contained in the anionic products. For example, the anion yield as a function of electron energy can be analysed to provide valuable information on the anion resonances, particularly when complementary data from vibrationally inelastic electron scattering are available,[33, 34, 35, 36, 37, 38, 39, 40, 41, 42, 43] or, in the case of electronic Feshbach resonances, photoelectron spectroscopy,[44] photoabsorption or electron energy loss spectroscopy[45] often allow identification of the parent excited electronic states states.

Experimental measurement of anion momentum distributions of DEA were first performed in the early 1970s by Van Brunt and Kieffer [9, 10] and Hall *et al.*[11, 12] using crossed-beam and angle- and kinetic energy-selective techniques. These pioneering experiments enabled crucial tests for development of theory to understand dissociative electron attachment electronic and nuclear dynamics. The development of 2-dimensional[46, 20] and 3-dimensional[47, 17, 16] ion imaging techniques over the subsequent years revolutionised the parallel detection of ions dispersed in space and time, enabling ions to be measured with large angle and energy acceptance intervals in parallel, while simultaneously resolving their momenta. Early experiments exploiting these developments to study DEA were performed by the groups of Krishnakumar[48, 49, 50], using velocity slice imaging[21] and Belkacem[51], using a reaction microscope[18], who adapted the techniques of COLTRIMS[17] for

anions. Subsequently, related experimental approaches have been developed by other groups in England[52], China[53], USA[19], India[54] and Germany[55]. The momentum imaging techniques established by these groups all employ a negative ion spectrometer that disperses the ion momentum distribution onto a large-area position-sensitive detector.

2.1. Momentum imaging

The LBNL DEA reaction microscope[18] consists of a pulsed electron gun that intersects orthogonally with a collimated effusive gas target. The first electrode of the anion spectrometer is typically pulsed following a few 100 ns delay from the electron gun pulse, extracting a negative ion fragment into the spectrometer following each DEA reaction, at a system repetition rate of typically 50 kHz. Maintaining an electron beam energy width ($\sim$0.5 eV) limited by the cathode temperature, each electron pulse is typically 50 ns in duration and consists of about 10^6 electrons. For a relatively dense ($\sim 10^{15}$molecules/cm^3) effusive target with a large resonant DEA cross section ($\sim 10^{-16}$ cm^2) such as water, the resulting total anion fragment detection rates will exceed 10 kHz. A magnetic field coaxial to the electron gun must be employed to allow efficient separation of anions from the scattered electron background and to assist with the low energy electron beam transport and collimation.

The COLTRIMS-type anion spectrometer (Fig. 1)consists of a series of resistively-coupled electrodes with an 80 mm circular opening. The ion extraction and acceleration fields, typically 12 V/cm, are followed by a position focusing lens before a field free drift region, such that the anion fragment trajectories originating from different positions within the intersection of the electron and molecular beams are focused to a much smaller area on the detector. Extensive shielding of the detector and spectrometer prevents most of the background scattered and secondary electrons from entering the spectrometer to arrive at the large area detector. The detector consists of a grid electrode for anion post-acceleration before arriving at a pair of chevron microchannel plates that amplify each detected particle onto a two-layer delay line anode, allowing for the event-by-event acquisition of the 3-dimensional momentum of each ion, encoded in the time and position of each ion hit. In the list-mode data record, the 3-dimensional momentum of each and every ion fragments is stored, allowing for both on-the-fly and offline analysis. Further details can be found in Refs [18, 19, 55]. The advantage of this and related approaches include the complete 4π ion angular acceptance within a broad range of ion kinetic energies, allowing measurements of the ion fragment kinetic energy distribution and presentation of the 3-dimensional momentum distribution in 2 dimensions by appropriate weighting or slicing[18, 19, 56]. The high detection efficiency of these experiments are limited primarily by the number of electrode grids employed (typically 3, each with 80-85% transmission) and the efficiency of the detector (typically 50$\sim$60% for post-accelerated anions). All anion fragments can be recorded in parallel, for a given electron beam energy, allowing for a single energy acquisition times as short as few minutes and typically less than 24 hours.

Momentum imaging in three dimensions also allows for a detailed analysis of systematic effects such as electric and magnetic field inhomogeneities or non-uniform detection efficiency. For randomly oriented target molecules, the cylindrical symmetry of the experiment about the electron beam axis can be exploited to extract accurate ion distributions. Anion kinetic energy and angular distributions can be extracted

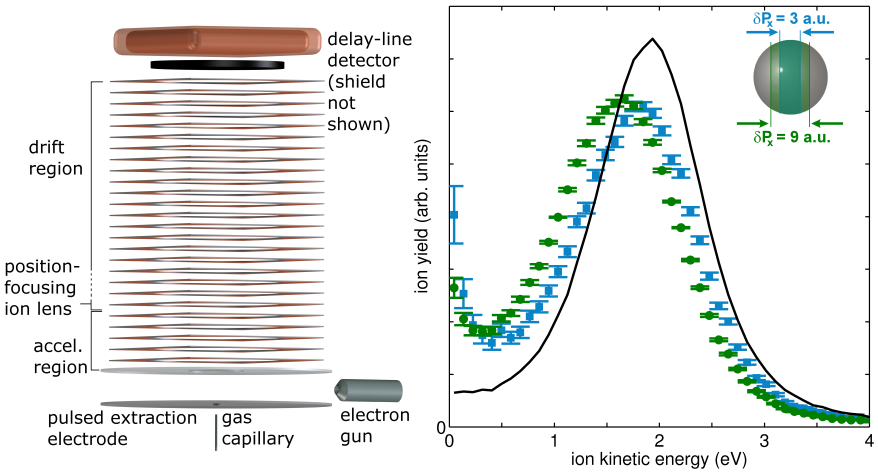

Figure 1. Left: A schematic illustration of the LBNL DEA reaction microscope. Right: Measured H^- kinetic energy distributions from DEA to H_2O at 6.3 eV, for different 3-dimensional momentum image analysis treatments illustrated inset. Solid curve: full 4π acceptance of the anion distribution; blue squares and green circles: slices parallel to the electron beam, selecting a fraction of the total H^- distribution (3 a.u. and 9 a.u. wide, respectively) about the center of the measured 3-dimensional image, demonstrating one advantage of 3-dimensional imaging in directly and accurately measuring the kinetic energy distribution. Further details can be found in Ref. [18]

.

with negligible corrections for the instrument function by either including the entire momentum space of an anion fragment, binning events with constant volume in momentum space, or slicing the distribution in momentum space while accounting for any change in that volume. One example in Fig. 1 illustrates the erroneous increase in ion events with low kinetic energy and corresponding shift in the peak kinetic energy when a subset of the ion distribution is selected about a plane through the center of the momentum distribution. While an appropriate inverse instrument function could be applied to the data to correct for this issue, 3-dimensional momentum imaging allows one to avoid these effects altogether.

2.2. Other approaches to imaging DEA

In the velocity slice imaging methods of Krishnakumar[21], Nandi[54] and Tian *et al.*[22], a time-gated subset of a mass-specific 3-dimensional anion fragment momentum distribution is measured on a 2-dimensional detector. Depending on the type of detector, these experiments allow the ion hit data to be stored either event-by-event or frame-by-frame, where one frame is an integration of many events. The advantage of the latter approach to acquiring anion fragment images is that the event rate per ion extraction pulse can be higher, possibly only limited by detector saturation, whereas event-by-event acquisition is generally more severely limited by the detector and acquisition system capabilities[57]. If a position- and time-sensitive detector is used[54], multiple anion fragments can readily be recorded in parallel, however the detection rate is then limited by the detector readout as is the case for the three-

dimensional momentum imaging experiments described above.

3. Theoretical approach

3.1. Nuclear wave equation

Dissociative electron attachment (DEA) is a resonant process in which a free electron is captured by a target N-electron molecule into a transient (N+1)-electron anion state. DEA occurs when this complex can form electronically stable (negative ion + neurtral) fragments before the transient anion can autodetach. The process can be treated using formal resonance theory, as formulated in the 1960's by O'Malley [15] and by Bardsley [14]. Using that formal theory, one finds that the equation which describes the relative nuclear motion of the nuclei in the transient anion state takes the form of a driven Schrödinger equation:

$$(E - H_{eff})\xi_i(\vec{Q}) = \phi_i(\vec{Q})\,, \tag{2}$$

where the nuclear degrees of freedom in the center-of-mass system are collectively denoted by $\vec{Q}$ and i is used to denote the initial state of the target. The term $\phi_i(\vec{Q})$ represents the coupling between the resonance state and the background continuum into which it can decay. If we assume that the adiabatic nuclei approximation is valid for the background (nonresonant) scattering [58], then $\phi_i(\vec{Q})$ can be factored as

$$\phi_i(\vec{Q}) = V(\vec{Q})\chi_i(\vec{q})\,, \tag{3}$$

where $\chi_i(\vec{q})$ is the initial rovibrational state of the target, which depends only on the internal degrees of freedom of the molecule $\vec{q}$, which are a subset of $\vec{Q}$. The quantity $V(\vec{Q})$, called the "entrance amplitude", is a matrix element of the electronic Hamiltonian H_{el} between the resonance state $\Psi_r(\vec{r},\vec{q})$ and the background state $P\Psi(\vec{r},\vec{Q})$:

$$V(\vec{Q}) = [\Psi_r(\vec{r},\vec{q})H_{el}P\Psi(\vec{r},\vec{Q})]\,. \tag{4}$$

The brackets in Eq. 4 denote integration only over electronic coordinates. It is important to note that the entrance amplitude depends not only on the internal nuclear coordinates $\vec{q}$ but also, through $P\Psi(\vec{r},\vec{Q})$, on the orientation of the molecule relative to the incident electron direction. As we will show below, this latter dependence, which is often ignored in computing total cross sections, is crucial in determining the angular dependence of DEA.

3.2. Local complex potential model

The Hamiltonian H_{eff} that appears in the nuclear wave equation of the formal theory (Eq. 2) is a complex-valued, non-local operator. It has formed the basis of the so-called non-local resonance model [59] and has been extensively applied to resonant vibrational excitation and DEA of various diatomic targets where only a single nuclear degree of freedom is involved. It has also been applied, as a semi-empirical model, to polyatomic targets by restricting the nuclear dynamics to a single dissociative coordinate. To our knowledge, the non-local theory has yet to be applied in any *ab initio* calculation with more that a single active nuclear coordinate. To make the latter computationally tractable, the nuclear wave equation must be further simplified. That simplification is offered by the local complex potential model.

In the local complex potential (LCP) model, which is also known as the "boomerang" model when applied to resonant vibrational excitation [60], the non-local Hamiltonian of the formal theory is approximated by a complex local operator, H_{lcp}:

$$H_{lcp} = T_{\vec{Q}} + E_R(\vec{q}) - \frac{i\Gamma(\vec{q})}{2}\,, \tag{5}$$

where $T_{\vec{Q}}$ is the nuclear kinetic energy operator and $E_R(\vec{q}) - i\Gamma(\vec{q})/2$ is the electronic energy of the resonance, whose width is Γ and whose real part is E_R.

The approximations made in deriving the local complex model and the conditions required for its validity have been thoroughly discussed in the literature [61, 62] and will not be repeated here. Suffice it to say that the conditions are well met for isolated resonances that can be described using the Born-Oppenheimer approximation, when said resonances do not lie too close (< 2eV) to electronically open channel thresholds and when the nonresonant background scattering can be described using the adiabatic nuclei approximation. The driven equation that defines the LCP model is then given by

$$\left(E - T_{\vec{Q}} - E_R(\vec{q}) + \frac{i\Gamma(\vec{q})}{2}\right)\xi_i(\vec{Q}) = V(\vec{Q})\chi_i(\vec{q})\,. \tag{6}$$

When only one nuclear degree of freedom is involved, Eq. 6 can be easily solved in coordinate space using standard numerical methods. When multiple dimensions are involved, we find that an equivalent time-dependent representation [63] is more efficient.

The LCP equation may be formally inverted,

$$\xi_i(\vec{Q}) = G^+(E)V(\vec{Q})\chi_i(\vec{q})\,, \tag{7}$$

where $G^+(E)$ is the Green's function,

$$G^+(E) = (E - H_{lcp} + i\epsilon)^{-1}. \tag{8}$$

The Green's function can be formally written as the Fourier transform of the propagator:

$$G^+(E) = \lim_{\epsilon\to 0} i\int_0^\infty dt\, e^{i(E+i\epsilon)t}e^{-iH_{lcp}t}\,, \tag{9}$$

giving

$$\begin{aligned}\xi_i(\vec{Q}) &= \lim_{\epsilon\to 0} i\int_0^\infty dt\, e^{i(E+i\epsilon)t}e^{-iH_{lcp}t}\phi_i(\vec{Q}) \\ &\equiv \lim_{\epsilon\to 0} i\int_0^\infty dt\, e^{i(E+i\epsilon)t}\psi_i(\vec{Q},t)\,,\end{aligned} \tag{10}$$

where we have defined the time-dependent wavepacket,

$$\psi_i(\vec{Q},t) = e^{-iH_{lcp}t}\phi_i(\vec{Q})\,, \tag{11}$$

whose value at time $t = 0$ is simply the driving term of the LCP equation. The essence of the LCP model is that the dynamics of this wavepacket on the complex potential surface of the metastable anion determines the cross section for dissociative attachment. The presence of the rovibrational target state $\chi_i(\vec{q})$ in $\phi_i(\vec{Q})$ makes the wavepacket square integrable. Moreover, because the complex Hamiltonian in the propagator has a negative imaginary part, the wavepacket vanishes at long times and the $i\epsilon$ in Eq. 10 can be dropped.

3.3. DEA cross sections and angular distributions

The entrance amplitude ties the body-frame of the target molecule to the laboratory-frame through the dependence of the background scattering wave function on the orientation of the molecule with respect to the incident electron. It is worth noting that this dependence is often ignored, when only integral cross sections are being calculated, by using Fermi's golden rule to approximate the entrance amplitude with the real quantity:

$$V(\vec{Q}) \approx \sqrt{\frac{\Gamma(\vec{q})}{2\pi}} \tag{12}$$

which ignores the dependence of the entrance amplitude on the laboratory-frame orientation of the target. In many other cases, the dynamics is simplified by assuming the entrance amplitude depends on a single partial wave [62, 64]. These simplifications are usually employed when the only resonance parameters available are the resonance position and lifetime. On the other hand, when resonance parameters are extracted from *ab initio* fixed-nuclei electron-molecule scattering calculations, which provide partial-wave $T-$ or $S-$ matrices, we can use formal resonance theory to extract the full laboratory-frame dependence of the entrance amplitude [65].

In the vicinity of a narrow resonance, we use the fact that the $S-$matrix can be symmetrically factored into background S^{bg} and resonant S^{res} components [66, 67]

$$\begin{aligned} S(e) &= S^{bg} S^{res} \\ &= S^{bg\,1/2}(E) \left(1 - \frac{iA}{E - E_r + i\Gamma/2}\right) S^{bg\,1/2}(E)\,, \end{aligned} \tag{13}$$

where S^{bg} is assumed to vary slowly with energy and A is a rank 1 matrix. Unitarity of S^{res} requires A to be Hermitian. Time-reversal invariance also requires the S-matrix to be symmetric and thus A to be real. In a partial-wave representation, we can thus write

$$A^{\Lambda\Lambda'}_{lm,l'm'} = \delta^{\Lambda}_{lm}\delta^{\Lambda'}_{l'm'}\,, \tag{14}$$

where Λ labels an electronically open channel.

Computationally, it is convenient to rewrite Eq. 13 as a sum:

$$S = S^{bg} + B\,, \tag{15}$$

where the matrix B is given by

$$B = -i\frac{S^{bg/,1/2}\,A\,S^{bg/,1/2}}{E - E_r + i\Gamma/2}\,, \tag{16}$$

with elements

$$\begin{aligned} B^{\Lambda\Lambda'}_{lm,l'm'} &= -i\frac{S^{bg\,1/2}\delta^{\Lambda}_{lm}\delta^{\Lambda'}_{l'm'}S^{bg\,1/2}}{E - E_r + i\Gamma/2} \\ &= -i\frac{\gamma^{\Lambda}_{lm}\gamma^{\Lambda'}_{l'm'}}{E - E_r + i\Gamma/2}\,. \end{aligned} \tag{17}$$

The background S-matrix has been incorporated into the quantities γ^{Λ}_{lm}, which are *complex* partial widths describing decay of the resonance into the physical channels labelled by (Λ, l, m). Note that because of the energy dependence of the background eigenphases, the partial widths are, in principal, energy dependent. However, because the magnitude of B is strongly peaked in the energy range $E_R - \Gamma/2 < E < E_R + \Gamma/2$

and Γ is small by assumption, we can assume the partial widths to be constant, ie. that $\gamma^{\Lambda}_{lm}(E) \approx \gamma^{\Lambda}_{lm}(E_R)$. Unitarity of S then demands that [68]

$$\Gamma = \sum_{\Gamma,l,m} |\gamma^{\Lambda}_{lm}|^2 \,. \tag{18}$$

We thus obtain, in the partial-wave representation, the following expression for the entrance amplitude $V^{\Lambda}(\vec{Q})$ of the LCP equation for electrons incident on the molecule in initial electronic state Λ:

$$V^{\Lambda}(\vec{Q}) = \sum_{l,m} i^l \gamma^{\Lambda}_{lm}(\vec{q}) Y^*_{lm}(\theta,\phi) \,, \tag{19}$$

where θ and ϕ define the direction of the incident electron with respect to the target. It is convenient to take the body-frame z-axis to coincide with the recoil axis, so that θ and ϕ represent the orientation of the incident electron relative to the dissociation axis in the molecular frame.

The computational procedure for determining the full set of parameters needed to determine the entrance amplitude, at a given nuclear geometry, proceeds in three steps:

1. Fixed-nuclei electron-molecule scattering calculations to obtain the multi-channel $S-$matrix. For this step, we use the complex-Kohn variational method [69, 70].
2. Fit the eigenphase sum to a Breit-Wigner form to obtain the resonance position E_R and width Γ.
3. Obtain the partial widths γ^{Λ}_{lm} by fitting the $S-$matrix to Eqs. 15 and 16, with E_R and Γ fixed using values from step 2. Eq. 18 is not imposed in the fitting, but rather used to gauge the overall accuracy of the fit.

We can summarise at this point to give an expression for the wavefunction $\xi^{\Lambda}_i(\vec{Q})$, which is exact within the adiabatic nuclei approximation and the assumptions leading to the LCP model:

$$\begin{aligned} \xi^{\Lambda}_i(\vec{Q}) &= i \int_0^{\infty} dt\, e^{i(E - H_{lcp}(\vec{Q}))t} V^{\Lambda}(\vec{Q}) \chi_i(\vec{q}) \\ &= i \int_0^{\infty} dt\, e^{i(E - H_{lcp})t} \chi_i(\vec{q}) \sum_{l,m} i^l \gamma^{\Lambda}_{lm}(\vec{q}) Y^*_{lm}(\theta,\phi) \,. \end{aligned} \tag{20}$$

It is worth noting that the solution of Eq. 20 requires knowing the resonance anion potential surface over the space of nuclear coordinates, in particular over the region where $\Gamma(\vec{q})$ is nonzero and the potential surface therefore complex. Moreover, since the function χ_i and the partial widths γ^{Λ}_{lm} both depend on the internal nuclear geometry, the LCP equation must be solved for every partial wave to obtain the angular dependence of the DEA cross section. Such a procedure was used in our earlier *ab initio* study of DEA to H_2O and H_2S, where the multi-configuration time-dependent Hartree (MCTDH) method [71] was used to solve the LCP equation in three dimensions on a complex surface constructed with parameters derived from complex Kohn scattering calculations. To our knowledge, these are the only such calculations ever carried out at this level in full dimensionality.

3.4. Axial recoil and Franck-Condon approximations

While the LCP model can provide fully differential cross sections for DEA with polyatomic targets, its implementation requires detailed knowledge of the resonance anion potential surface, which is often beyond the scope of many theoretical investigations. The focus of most modern imaging investigations of DEA with polyatomic targets, however, is on angular distributions and not absolute integral or differential cross sections. In the favorable cases of prompt dissociation, characterised by the existence of predominant dissociation pathways, we have found that the entrance amplitude, which can be calculated with the full set of resonance parameters extracted from electron-molecule scattering calculations, can often explain observed angular distributions without recourse to a full solution of the LCP model and, when combined with electronic structure calculations, can tie the observations to specific dissociation mechanisms.

We proceed by noting that the driving term of the LCP equation in the adiabatic nuclei approximation, $V^{\Lambda}(\vec{Q})\chi_i(\vec{q})$, is factorable, but $V^{\Lambda}(\vec{Q})$ may nevertheless have a non-trivial dependence on the internal nuclear coordinates through the partial resonance widths $\gamma^{\Lambda}_{lm}(\vec{q})$. The nuclear coordinate space over which the partial widths are required, however, is confined by the initial target state to the Franck-Condon region. If the partial widths do not vary significantly over this region, then it may be reasonable to ignore their $\vec{q}$-dependence and replace them with $\gamma^{\Lambda}_{lm}(\vec{q_0})$, their value at the equilibrium geometry of the target. In earlier work, we termed this Franck-Condon-like approximation the "constant eigenmode" approximation. With this approximation, the entrance amplitude, which largely determines the magnitude of the DEA cross section through the LCP equation, becomes

$$V^{\Lambda}(\vec{Q}) \approx V^{\Lambda}_0 \equiv \sum_{l,m} i^l \gamma^{\Lambda}_{lm}(\vec{q_0}) Y^*_{lm}(\theta,\phi)\,. \tag{21}$$

The key point to note is that with this approximation the angular dependence of the cross section is determined by the entrance amplitude alone. That angular dependence is given by

$$\frac{d\sigma^{\Lambda}}{d\theta} \propto \int d\phi \left| \sum_{l,m} i^l \gamma^{\Lambda}_{lm}(\vec{q_0}) Y^*_{lm}(\theta,\phi) \right|^2 . \tag{22}$$

The integration over the angle ϕ azimuthal to the recoil axis is performed under the assumption that the relative orientation of the fragments is not observed.

One consequence of Eq. 22 is the prediction that the angular dependence of DEA is independent of the initial vibration state of the target. When this is not the case, as was found for H_2S, it signals a breakdown of the "constant eigenmode" approximation.

For Eq. 22 to be a good approximation, the axial recoil approximation must be satisfied, ie. there should be no internal rotation or bending of the transient ion before dissociation takes place. Nevertheless, as we have found in a number of previous studies, we may still be able to use the computed entrance amplitudes to predict angular distributions in cases where axial recoil fails if we have theoretical evidence that points to how the recoil axis changes following electron attachment. We have found that we may still be able to reasonably predict the angular distributions by simply rotating the entrance amplitude to the appropriate recoil frame before

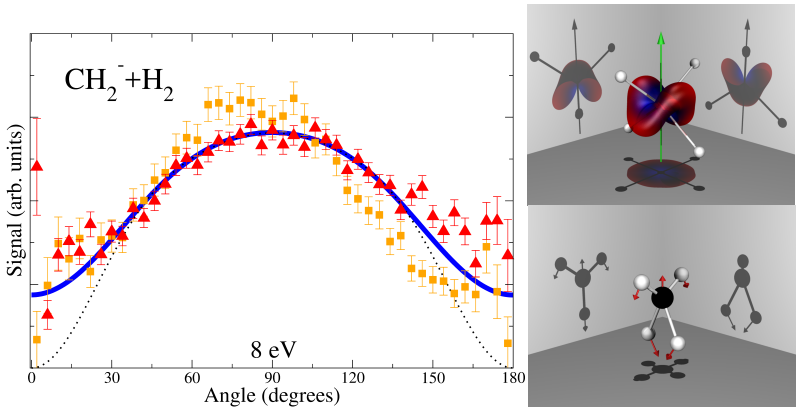

Figure 2. Measured CH_2^- (squares) and CD_2^- (triangles) angular distributions (left) from DEA to CH_4 and CD_4, respectively, at 8 eV, compared with the axial recoil theoretical prediction (dashed curve) and the recoil-averaged theoretical prediction (solid curve) based on the complex Kohn variational method. Also shown are the square of the electron attachment entrance amplitude for the T_x and T_y components of the $^2T_2$ resonance (top-right), with the green arrow indicating the asymptotic recoil direction, and an illustration of the relevant molecular geometries leading to the dissociation (bottom-right) from the same work. Reproduced from Ref. [72] with permission from the PCCP Owner Societies.

computing the angular distributions. This rotation can be carried out analytically with the transformation

$$\gamma^{\Lambda}_{lm}(\vec{q}_0) \rightarrow \sum_{m'} D^{J}_{m'm}(\alpha,\beta,\gamma)\gamma^{\Lambda}_{lm'}(\vec{q}_0)\,, \tag{23}$$

where α, β, γ are the Euler angles which orient the molecule in the new coordinate system.

4. Examples

4.1. Transient anion isomerisation and rearrangement

There are numerous examples of electron attachment to a polyatomic target leading to different ionic fragments through both bond dissociation and bond formation channels; in many such cases[8, 73, 74] these dynamics have been identified solely by the electron energy - dependent anion fragment mass spectra. Analysis of the kinetic energy release in the dissociation lends unique information on these dynamics that may not be retrieved by mass spectrometry alone. Our recent study of DEA to methane provides an interesting example. DEA in methane proceeds through three prominent dissociation channels [75],

$$\begin{aligned} e^- + CH_4 \rightarrow CH_4^- &\rightarrow H^- + CH_3 && (a)\\ &\rightarrow H_2 + CH_2^- && (b)\\ &\rightarrow H^- + H + CH_2 \ , && (c) \end{aligned} \tag{24}$$

all observed to proceed from a broad dissociation peak, extending from 8 to 12 eV and centered at about 10 eV electron energy. Douguet *et al.*[72] have shown that

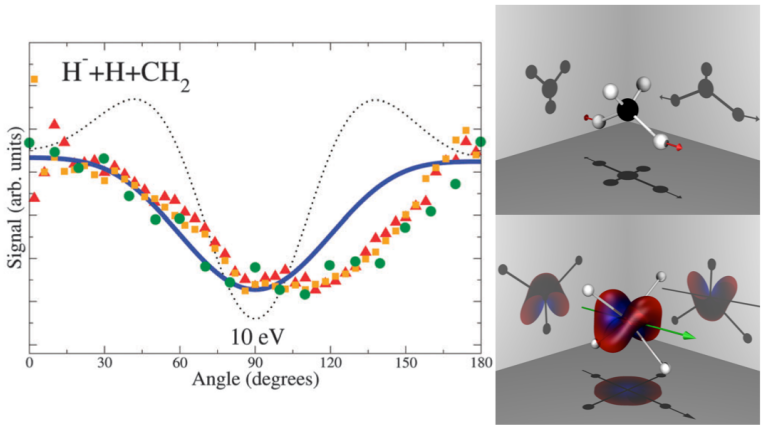

Figure 3. Angular distributions for 3-body breakup channel from DEA to CH_4 and CD_4 at 10 eV. Green circles are from ref. [75]. All other data labeled as in Fig. 2. Reproduced from Ref. [72] with permission from the PCCP Owner Societies.

electron capture to a single triply degenerate (T_2) Feshbach resonance is responsible for all three breakup channels. The assignments were based on analysis of the anion fragment momentum distributions and *ab initio* calculations of the topology of the anion potential energy surface. For example, the two-body channel involving dihydrogen bond formation (Eq. 24b) is a consequence of the stretch of two C-H bonds combined with closure of the H-C-H angle between them (see Fig. 2), while the three-body breakup channel (Eq. 24c) is the result of simultaneous stretching of two CH bonds (see Fig. 3).

It is important to bear in mind that the observed width of the DEA peak (∼4 eV) is a reflection of how the Franck-Condon window of the neutral target projects onto the dissociative anion surface and is not determined by the intrinsic fixed-nuclei electronic width of the resonance. The latter has a magnitude of only several meV. This narrow width translates to a long lifetime against electron autodetachment and thus allows the initially created wavepacket to explore different regions of the anion potential energy surface. The calculated angular distributions for the various breakup channels were all generated from the same entrance amplitude, but using different choices for the recoil axis.

The competition between two-body and three-body breakup to produce $H^-(D^-)$ displays an interesting isotope effect, as shown in the contrasting momentum images of Fig. 4. Three-body dissociation has a thermodynamic threshold of at least 8.37 eV, while the two-body channel threshold is some 5 eV smaller. At 8.5 eV electron energy, the two-body channel ($H^-(D^-)$ + CH_3), corresponding to the outer ring in the momentum plots, dominates both H^- and D^- production; the three-body breakup

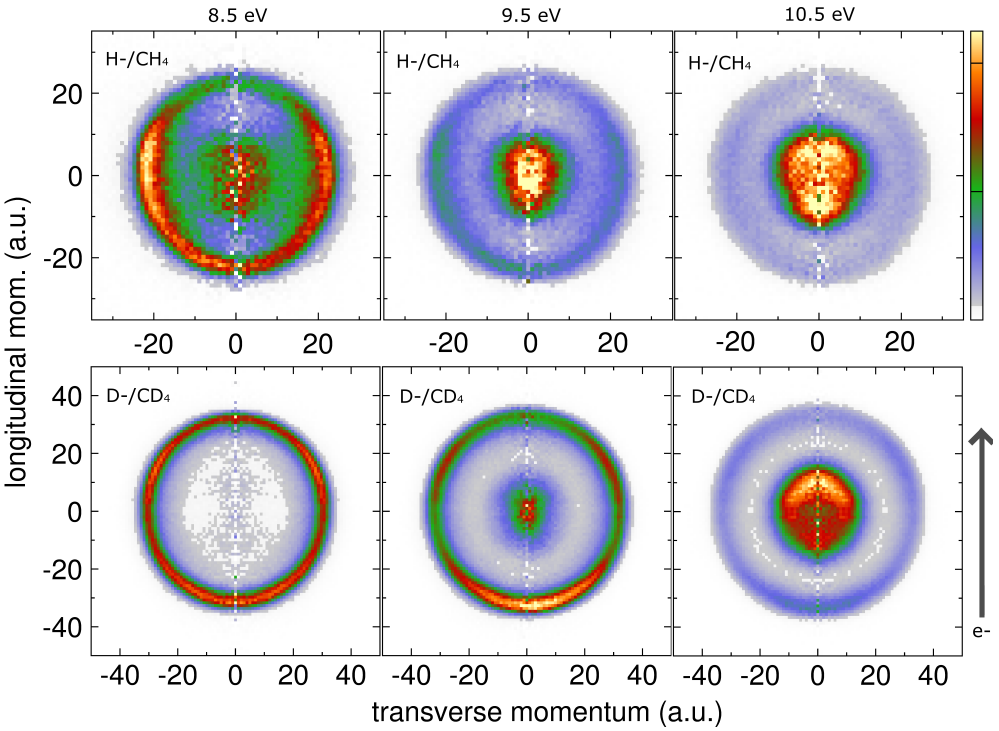

Figure 4. Measured H^- (top row) and D^- (bottom row) momentum images for DEA to CH_4 and CD_4, respectively, at 8.5 eV (left column), 9.5 eV (center column) and 10.5 eV (right column). The outer ring that is dominant at lower electron attachment energy is due to two-body dissociation while the inner peak that is dominant at higher electron attachment energy is due to three-body dissociation. The vertical arrow denotes the incident electron direction. Further details can be found in Ref. [72].

channel, corresponding to the inner ring in the momentum plots, is barely visible in the three-body D^- channel. As the electron energy increases, so does the ion kinetic energy and the three-body D^- intensity increases correspondingly. While the two-body ion channel is a direct process involving a single bond stretch, the internal rearrangement required for three-breakup is a concerted motion involving all four bonds (see Fig. 3) and is thus surpressed for the heavier deuterated molecule at low ion kinetic energies.

4.2. Conical intersections

A conical intersection is a set of molecular geometries where degeneracies couple two or more adiabatic electronic potential energy surfaces[76]. For molecular geometries near a conical intersection, the electronic and nuclear dynamics of the system become strongly coupled by non-adiabatic transitions. These phenomena can strongly influence the outcomes of reactions and, by violating the Born-Oppenheimer Approximation, present severe limitations on quantum chemical calculations of the molecular dynamics in these systems. Numerous experimental studies of anion production from DEA resonances in polyatomic molecules have shown that more than

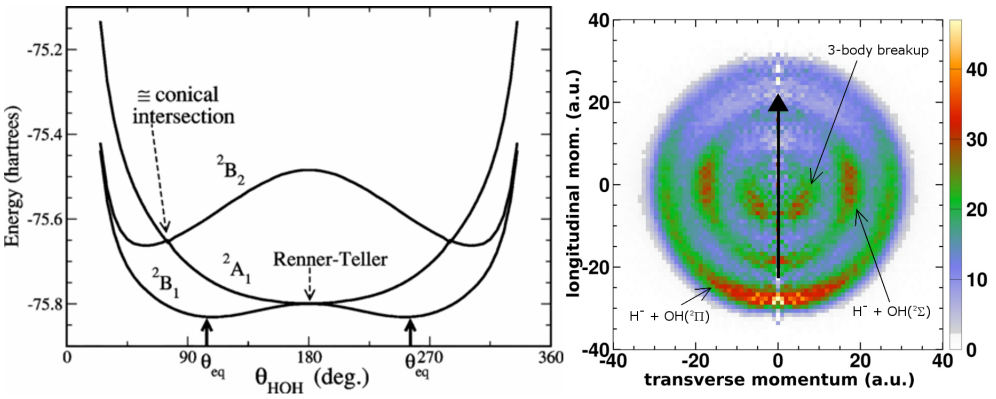

Figure 5. Left: HOH angle dependence of the real parts of resonance energies of three states of the H_2O anion, for OH bond distance=1.81a_0, in C_{2v} geometry from a four-configuration multi-configuration self consistent field calculation, from Ref. [80]. Right: H^- momentum distribution (a.u.: atomic units) following DEA to water at 11.3 eV. The peaks in the distribution are due to three dissociation channels, as labeled. The electron direction is indicated by a vertical arrow. From Refs [77] and [80].

one anionic fragment is typically produced from each resonance, therefore it is likely that non-adiabatic transitions including conical intersections are ubiquitous in the dissociation dynamics of polyatomic anions. Recent momentum imaging studies of the dynamics of DEA have enabled conical intersections between electronic states of anions to be explicitly identified in a few relatively small molecules[77, 78, 79].

To date, there are perhaps no electron-molecule systems as comprehensively studied as the transient anions of water participating in DEA. Momentum imaging studies were combined with theoretical calculations of the electron attachment amplitude and dissociation dynamics[51, 77] allowing a detailed investigation of conical intersections between electronic states of the transient water anion. The water anion can be formed by any of three Feshbach resonances $^2B_1$, $^2A_1$ and $^2B_2$ for electron attachment energies around 6.5 eV, 9 eV and 12 eV, respectively. Haxton *et al.* showed that these states are coupled[80, 81] by a conical intersection and the Renner-Teller effect[82].

In the lowest energy resonance at 6.5 eV, the angular distribution of the products H^- and OH are well described by the axial recoil approximation and the cross section and fragment kinetic energy are well described by a local complex potential model using the Multi-Configuration Time-Dependent Hartree Fock (MCTDHF) method[83]. This state contrasts dramatically with the higher two Feshbach resonances $^2A_1$ and $^2B_2$, having attachment energies of approximately 8.5 eV and 12 eV, respectively, which are electronically coupled by a conical intersection[80, 81, 77]. This manifests experimentally as the production of comparable quantities of electronically excited OH($^2\Sigma$), by the dissociating wavepacket of the $^2B_2$ resonance avoiding the conical intersection, and the electronic ground state OH($^2\Pi$) due to the wavepacket passing through the conical intersection (Fig. 5).

Another triatomic electron-molecule system that has been the subject of intense study is the carbon dioxide anion. DEA to carbon dioxide can proceed *via* two low energy resonances: one at 4 eV is a shape resonance of $^2\Pi_u$ symmetry that has been

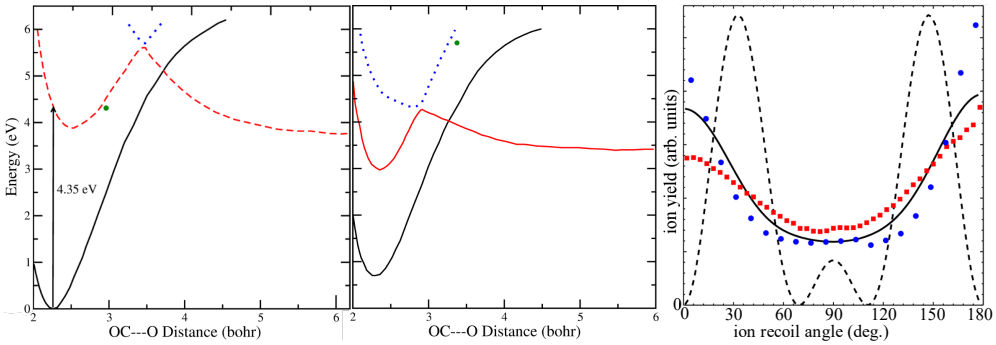

Figure 6. Potential curves of neutral CO_2 and the shape- and Feshbach anion states, showing the avoided crossing between the two resonance states from Ref. [78]. Left: Linear geometry; the point near 3 bohr shows the position of the crossing when the OCO angle is 140°. Middle: OCO angle is 140°; the point near 3.4 bohr shows the position of the crossing when the OCO angle is 180°. Right: O^- angular distributions from two independent COLTRIMS measurements, compared with axial recoil prediction (solid curve) and recoil-averaged prediction.

studied extensively by electron scattering[84, 85, 86, 34, 35, 38, 39, 40, 41, 42, 43] and DEA[36, 87, 88, 89, 90, 37, 91, 92, 93, 94, 33, 78, 53, 54]. A second resonance occurs in DEA at electron impact energies near 8 eV[36, 87, 90, 91, 92, 93, 94, 33, 53, 54, 95, 56, 96]. This Feshbach resonance is understood to have a long autodetachment lifetime, such that the anion preferentially dissociates and the resonance is less prevalent in electron scattering cross sections[97, 86, 98]. As shown by the calculated cuts through the CO_2^- potential energy surfaces in Fig. 6, the two resonances dissociate to the same electronic ground state products $CO(^1\Sigma^+) + O^-(^2P)$ and couple at bent and stretched geometries by conical intersections[78]. These predictions were supported by experiments at LBNL and Auburn University: the axial recoil prediction was averaged over a broad range of recoil angles to simulate bending in the dissociating anion, producing good agreement with the measured O^- angular distributions.

4.3. Charge exchange between dissociating fragments

We have discussed several examples where DEA to a polyatomic target can involve different ion fragmentation channels. In some cases, such as methanol, the different channels represent different asymptotes on a single anion surface. In other cases, such as water , carbon dioxide and methanol [99], conical intersections between different anion surfaces are implicated in the dynamics. In the case of the ammonia molecule, we find a different breakup mechanism. The 5.5 eV resonance in NH_3 feeds two different fragmentation channels:

$$\begin{aligned} e^- + NH_3 \rightarrow NH_3^- &\rightarrow H^- + NH_2 \ (a) \\ &\rightarrow H + NH_2^- \ .(b) \end{aligned} \tag{25}$$

The interesting point to note is that the two asymptotic channels are almost degenerate, with the H^-+NH_2 lying only 0.02 eV above the H+NH_2^- asymptote. Theory shows that the 5.5 eV resonance is a non-degenerate $^2A'$ state that correlates with the H^- asymptote. The lower NH_2^- asymptote does not connect to any resonance

state, but rather decreases in energy as the NH_2–H distance decreases and becomes a virtual state at small separations. The two anion surfaces do not cross, but rather parallel each other at large distances. We conclude that the NH_2^- asymptote must be populated by a non-adiabatic charge-exchange mechanism between the two anion surfaces that takes place at large distances. This was confirmed by time-dependent wavepacket calculations that reproduce the observed branching ratios. Since the charge-exchange takes place at large separations, the short-time dynamics that determines the angular distributions takes place on the $^2A'$ surface. Indeed, the measured angular distributions for H^-+NH_2 and H+NH_2^- are related by reflection through 90 degrees [79].

There is a second 10 eV resonance peak in ammonia which predominately (∼85 percent) feeds an H^- + NH_2* channel, with smaller amounts of NH_2^- + H. The measured ion kinetic energy for the resonance points to NH_2 being produced in its excited $^2A_1$ state, which is confirmed by theory. The small observed yield of NH_2^- is difficult to explain. The NH_2^- momentum distribution appears to be a mirror image of the H^- distribution (see Fig. 7), strongly suggesting that the two channels are produced from the same 10 eV resonance and therefore the same electron attachment entrance probability. Structure calculations do not serve to identify any negative ion state that could connect the upper (^2E) resonance state to either the lower $^2A'$ resonance surface or the virtual state. It is possible that a broad 10 eV shape resonance observed in elastic scattering [100] could provide a coupling between the upper and lower resonances, the latter then populating the NH_2^-+H channel through the same charge-exchange mechanism previously discussed.

4.4. Electron-driven chemistry in molecules of biological and technological significance

Molecular systems with relatively large size and complexity pose significant challenges for experimental investigations of DEA reactions that rely on detection of a single fragment. Even in favorable reactions leading to two-body dissociation, fragments of these systems can possess many internal degrees of freedom that can become excited while remaining indistinguishable in the final anion fragment momentum. Furthermore, warm polyatomic molecules undergo conformational changes[102, 103] and, in many cases tautomerisation, compounding any accurate description of the experimental target unless considerable vibrational cooling is performed. Uracil is one relatively favorable system that has essentially one geometry[104, 105] at temperatures that establish a sufficient vapor pressure for a gas target. Recent investigations of this system by a variety of experimental techniques[106] established a remarkable site-selectivity despite the predominantly slow metastable decomposition that dominates in the production of the major anionic fragment NCO^-. A subsequent momentum imaging study[107] revealed dynamical information for resonances at 6 eV, characterising several pathways comparable to the slow decomposition in addition to two fast dissociation pathways resulting in H^- loss and H+CO loss.

5. Conclusions and outlook

These recent advances in momentum imaging techniques have provided crucial information to describe the transient anion dynamics of DEA. The kinetic energy- and angle-resolved measurements that we have reviewed here were transformed to

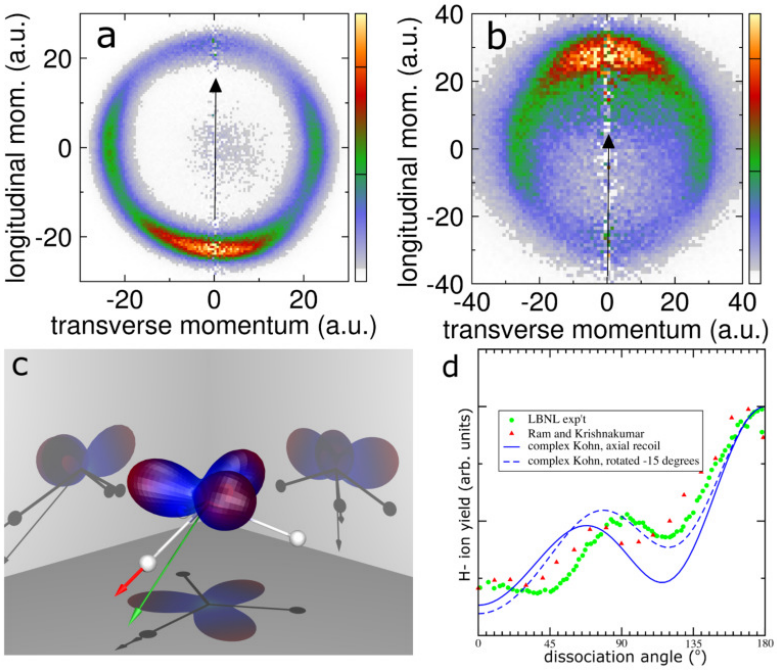

Figure 7. Measured momentum distributions of H^- (panel a) and NH_2^- (panel b) following dissociative electron attachment to ammonia. The arrows illustrate the incident momentum direction and the intensity scale is the ion yield in arbitrary units. Panel c: entrance probability in the NH_3 molecular frame. The red arrow depicts the recoil axis and the green arrow is the recoil axis after a 15° rotation. Panel d: Measured H^- angular distribution of Resigno *et al.* [79] (circles) and Ram and Krishnakumar[101] (triangles). The solid and dashed curves are the complex Kohn calculation of the ion trajectory following axial recoil conditions and a 15-degree rotated axis, respectively. From Ref. [79].

the molecular frame with the aid of the calculated electron attachment entrance amplitude, allowing dissociation dynamics to be explored well-beyond the axial recoil approximation. The result is a powerful guide for directing quantum chemistry calculations of the anion potential energy surfaces that would otherwise be computationally intractable.

Several opportunities exist to extend these techniques by laser preparation of target excited states, including vibrational or electronic excitation and adiabatic or impulsive alignment or orientation [108] of the target molecule before electron attachment. Such experimental control of the ensemble of target molecules would allow the exploration of electron attachment processes away from the equilibrium geometry of the target molecule and new information on the dependence of the electronic dynamics in the molecular frame. Other potential extensions of momentum imaging techniques are in the direction of more complex systems, such as the exploration of the dynamics of dissociative electron attachment to Van Der Waals clusters[26, 25, 24] or to molecules within a nanoparticle or droplet[109]. Furthermore, many of the techniques that we have described could be employed to interrogate neutral fragments from electron attachment (also dissociative excitation or ionisation) by a suitable selective

ionisation scheme such as REMPI[110] or resonant single photon ionisation[111].

Acknowledgments

This work is supported by the U.S. DOE Office of Basic Energy Sciences, Division of Chemical Sciences, Geosciences and Biosciences under contract DE-AC02-05CH11231.

References

[1] Kushner M J 2009, *Journal of Physics D: Applied Physics* **42**(19) 194013
[2] Perry C C, Wolfe G M, Wagner A J, Torres J, Faradzhev N S, Madey T E and Fairbrother D H November 2003 *The Journal of Physical Chemistry B* **107**(46) 12740–12751
[3] Utke I and Gölzhäuser A December 2010 *Angewandte Chemie International Edition* **49**(49) 9328–9330
[4] Abdoul-Carime H, Gohlke S and Illenberger E April 2004 *Physical Review Letters* **92**(16) 168103
[5] Ptasińska S, Denifl S, Grill V, Märk T D, Illenberger E and Scheier P August 2005 *Physical Review Letters* **95**(9) 093201
[6] Schulz G J July 1973 *Reviews of Modern Physics* **45**(3) 423–486
[7] Allan M January 1989 *Journal of Electron Spectroscopy and Related Phenomena* **48**(2) 219–351
[8] Oster T, Kühn A and Illenberger E April 1989 *International Journal of Mass Spectrometry and Ion Processes* **89**(1) 1–72
[9] Van Brunt R J and Kieffer L J November 1970 *Physical Review A* **2**(5) 1899–1905
[10] Van Brunt R J and Kieffer L J November 1974 *Physical Review A* **10**(5) 1633–1637
[11] Cadez I, Tronc M and Hall R I April 1975 *Journal of Physics B: Atomic and Molecular Physics* **8**(5) L73–L76
[12] Trajmar S and Hall R I November 1974 *Journal of Physics B: Atomic and Molecular Physics* **7**(16) L458
[13] Bardsley J N, Herzenberg A and Mandl F 1966 *Proceedings of the Physical Society* **89**(2) 321
[14] Bardsley J N 1968 *J. Phys.B: At. Mol. Phys.* **1**(3) 349
[15] O'Malley T F 1966 *Phys. Rev.* **150**(1) 14
[16] Ullrich J, Moshammer R, Dorn A, Dörner R, Schmidt L P H and Schmidt-Böcking H 2003 *Reports on Progress in Physics* **66**(9) 1463–1545
[17] Dörner R, Mergel V, Jagutzki O, Spielberger L, Ullrich J, Moshammer R and Schmidt-Böcking H June 2000 *Physics Reports* **330**(2-3) 95–192
[18] Adaniya H, Slaughter D S, Osipov T, Weber T and Belkacem A 2012 *Review of Scientific Instruments* **83**(2) 023106
[19] Moradmand A, Williams J B, Landers A L and Fogle M 2013 *Review of Scientific Instruments* **84**(3) 033104
[20] Chandler D W and Houston P L 1987 *The Journal of Chemical Physics* **87**(2) 1445
[21] Nandi D, Prabhudesai V S, Krishnakumar E and Chatterjee A 2005 *Review of Scientific Instruments* **76**(5) 053107
[22] Wu B, Xia L, Li H K, Zeng X J and Xi Tian S 2012 *Review of Scientific Instruments* **83**(1) 013108
[23] Illenberger E and Momigny J 1992 *Gaseous molecular ions an introduction to elementary processes induced by ionization* Steinkopff Verlag ; Springer-Verlag Darmstadt; New York
[24] Ingólfsson O, Weik F and Illenberger E October 1996 *International Journal of Mass Spectrometry and Ion Processes* **155**(1-2) 1–68
[25] Hotop H, Ruf M W, Allan M and Fabrikant I In *Advances In Atomic, Molecular, and Optical Physics* volume 49 85–216 Elsevier 2003
[26] Bald I, Langer J, Tegeder P and Ingólfsson O November 2008, *International Journal of Mass Spectrometry* **277**(1-3) 4–25
[27] McConkey J, Malone C, Johnson P, Winstead C, McKoy V and Kanik I September 2008 *Physics Reports* **466**(1-3) 1–103
[28] Böhler E, Warneke J and Swiderek P 2013 *Chemical Society Reviews* **42**(24) 9219
[29] Yamazaki M, Kasai Y, Oishi K, Nakazawa H and Takahashi M 2013 *Review of Scientific Instruments* **84**(6) 063105

[30] Yamazaki M, Oishi K, Nakazawa H, Zhu C and Takahashi M March 2015 *Physical Review Letters* **114**(10)
[31] Paarmann A, Gulde M, Müller M, Schäfer S, Schweda S, Maiti M, Xu C, Hohage T, Schenk F, Ropers C and Ernstorfer R 2012 *Journal of Applied Physics* **112**(11) 113109
[32] Gulde M, Schweda S, Storeck G, Maiti M, Yu H K, Wodtke A M, Schafer S and Ropers C July 2014 *Science* **345**(6193) 200–204
[33] Dressler R and Allan M January 1985 *Chemical Physics* **92**(2-3) 449–455
[34] Allan M 2002 *Journal of Physics B: Atomic, Molecular and Optical Physics* **35**(17) L387–L395
[35] Allan M June 2001 *Physical Review Letters* **87**(3) 033201
[36] Schulz G J October 1962 *Phys. Rev.* **128**(1) 178–186
[37] Stamatovic A and Schulz G February 1973 *Physical Review A* **7**(2) 589–592
[38] Vanroose W, McCurdy C and Rescigno T September 2002 *Physical Review A* **66**(3)
[39] Vanroose W, Zhang Z, McCurdy C and Rescigno T February 2004 *Physical Review Letters* **92**(5)
[40] T. Sommerfeld, H. -D Meyer and L. S. Cederbaum 2004 *Phys. Chem. Chem. Phys.* 42–45
[41] Rescigno T, Byrum D, Isaacs W and McCurdy C September 1999 *Physical Review A* **60**(3) 2186–2193
[42] Rescigno T, Isaacs W, Orel A, Meyer H D and McCurdy C February 2002 *Physical Review A* **65**(3)
[43] McCurdy C, Isaacs W, Meyer H D and Rescigno T April 2003 *Physical Review A* **67**(4) 042708
[44] Ibănescu B C, May O, Monney A and Allan M 2007 *Physical Chemistry Chemical Physics* **9**(24) 3163
[45] Curtis M G and Walker I C 1992 *Journal of the Chemical Society, Faraday Transactions* **88**(19) 2805
[46] Eres D, Gurnick M and McDonald J D 1984 *The Journal of Chemical Physics* **81**(12) 5552
[47] Ullrich J, Moshammer R, Dörner R, Jagutzki O, Mergel V, Schmidt-Böcking H and Spielberger L July 1997 *Journal of Physics B: Atomic, Molecular and Optical Physics* **30**(13) 2917–2974
[48] Prabhudesai V S, Nandi D and Krishnakumar E July 2006 *Journal of Physics B: Atomic, Molecular and Optical Physics* **39**(14) L277–L283
[49] Prabhudesai V S, Ram N B, Aravind G, Rawat P and Krishnakumar E September 2007 *Journal of Physics: Conference Series* **80** 012016
[50] Ram N B, Prabhudesai V S and Krishnakumar E November 2009 *Journal of Physics B: Atomic, Molecular and Optical Physics* **42**(22) 225203
[51] Adaniya H, Rudek B, Osipov T, Haxton D J, Weber T, Rescigno T N, McCurdy C W and Belkacem A November 2009 *Physical Review Letters* **103**(23) 233201
[52] Ómarsson F H, Szymanska E, Mason N J, Krishnakumar E and Ingólfsson O August 2013 *Physical Review Letters* **111**(6) 063201
[53] Wu B, Xia L, Wang Y F, Li H K, Zeng X J and Tian S X May 2012 *Physical Review A* **85**(5) 052709
[54] Nag P and Nandi D May 2015 *Physical Review A* **91**(5)
[55] Weyland M, Ren X, Pflüger T, Dornt A, Baek W Y and Rabus H September 2015 *Journal of Physics: Conference Series* **635**(7) 072013
[56] Moradmand A, Slaughter D S, Landers A L and Fogle M August 2013 *Physical Review A* **88**(2) 022711
[57] Jagutzki O, Cerezo A, Czasch A, Dorner R, Hattas M, Min Huang, Mergel V, Spillmann U, Ullmann-Pfleger K, Weber T, Schmidt-Bocking H and Smith G October 2002 *IEEE Transactions on Nuclear Science* **49**(5) 2477–2483
[58] Shugard M and Hazi A U November 1975 *Physical Review A* **12**(5) 1895–1902
[59] Domcke W 1991 *Phys. Rep.* **208**(2) 97
[60] Birtwistle D T and Herzenberg A 1971 *J. Phys. B: At. Mol. Phys.* **4**(1) 53
[61] Bieniek R J 1978 *Phys. Rev. A* **18**(2) 392
[62] Hazi A U, Rescigno T N and Kurilla M 1981 *Phys. Rev. A* **23**(3) 1089
[63] McCurdy C W and Turner J L 1983 *J. Chem. Phys.* **78**(11) 6773
[64] Dubé L and Herzenberg A 1979 *Phys. Rev. A* **20**(1) 194
[65] Haxton D J, McCurdy C W and Rescigno T N 2006 *Phys. Rev. A* **73**(6) 062724
[66] Brenig W and Haag R 1959 *Fortschr. Physik* **7** 183
[67] Macek J 1970 *Phys. Rev. A* **2**(3) 1101
[68] Taylor J R 1972 *Scattering Theory: The Quantum Theory of Nonrelativistic Collisions* John Wiley and Sons, Inc.

[69] Rescigno T N, Lengsfield B H and McCurdy C W In *Modern electronic structure theory,* Yarkony D R, editor volume I 501 World Scientific Singapore 1995

[70] Rescigno T N, McCurdy C W, Orel A E and Lengsfield B H In *Computational Methods for Electron-Molecule Collisions,* Huo W and Gianturco F, editors, 1 Plenum, New York 1995

[71] Beck M H, Jäckle A, Worth G A and Meyer H D 2000, *Phys. Repts.* **324** 1

[72] Douguet N, Slaughter D S, Adaniya H, Belkacem A, Orel A E and Rescigno T N 2015 *Phys. Chem. Chem. Phys.* **17**(38) 25621–25628

[73] Pariat Y and Allan M January 1991 *International Journal of Mass Spectrometry and Ion Processes* **103**(2-3) 181–192

[74] Ómarsson B and Ingólfsson O 2013 *Physical Chemistry Chemical Physics* **15**(39) 16758

[75] Ram N B and Krishnakumar E July 2011 *Chemical Physics Letters* **511**(1–3) 22–27

[76] Domcke W and Yarkony D R May 2012 *Annual Review of Physical Chemistry* **63**(1) 325–352

[77] Haxton D J, Adaniya H, Slaughter D S, Rudek B, Osipov T, Weber T, Rescigno T N, McCurdy C W and Belkacem A September 2011 *Physical Review A* **84**(3) 030701R

[78] Moradmand A, Slaughter D S, Haxton D J, Rescigno T N, McCurdy C W, Weber T, Matsika S, Landers A L, Belkacem A and Fogle M September 2013 *Physical Review A* **88**(3) 032703

[79] Rescigno T N, Trevisan C S, Orel A E, Slaughter D S, Adaniya H, Belkacem A, Weyland M, Dorn A and McCurdy C W May 2016 *Physical Review A* **93**(5) 052704

[80] Haxton D J, Rescigno T N and McCurdy C W August 2005 *Physical Review A* **72**(2) 022705

[81] Haxton D J, Rescigno T N and McCurdy C W January 2007 *Physical Review A* **75**(1) 012711

[82] Petrongolo C 1988 *The Journal of Chemical Physics* **89**(3) 1297

[83] Haxton D J, Zhang Z, Meyer H D, Rescigno T N and McCurdy C W June 2004 *Physical Review A* **69**(6) 062714

[84] Boness M and Schulz G May 1974 *Physical Review A* **9**(5) 1969–1979

[85] Burrow P D and Sanche L February 1972 *Physical Review Letters* **28**(6) 333–336

[86] Gianturco F A and Stoecklin T May 2001 *Journal of Physics B: Atomic, Molecular and Optical Physics* **34**(9) 1695–1710

[87] Rapp D and Briglia D D 1965 *The Journal of Chemical Physics* **43**(5) 1480–1489

[88] Bardsley J N 1969 *The Journal of Chemical Physics* **51**(8) 3384

[89] Schulz G J and Spence D January 1969 *Physical Review Letters* **22**(2) 47–50

[90] Chantry P J 1972 *The Journal of Chemical Physics* **57**(8) 3180

[91] Abouaf R, Paineau R and Fiquet-Fayard F February 1976 *Journal of Physics B: Atomic and Molecular Physics* **9**(2) 303

[92] Tronc M, Malegat L and Azria R 1982 *Chemical Physics Letters* **92**(5) 551–555

[93] Srivastava S K and Orient O J February 1983 *Phys. Rev. A* **27**(2) 1209–1212

[94] Orient O and Srivastava S April 1983 *Chemical Physics Letters* **96**(6) 681–684

[95] Sizun M and Goursaud S 1979 *J. Chem. Phys.* **71**(10) 4042–4049

[96] Slaughter D S, Adaniya H, Rescigno T N, Haxton D J, Orel A E, McCurdy C W and Belkacem A October 2011 *Journal of Physics B: Atomic, Molecular and Optical Physics* **44**(20) 205203

[97] Chantrell S J, Field D and Williams P I January 1982 *Journal of Physics B: Atomic and Molecular Physics* **15**(2) 309–318

[98] Itikawa Y September 2002 *Journal of Physical and Chemical Reference Data* **31**(3) 749

[99] Slaughter D S, Haxton D J, Adaniya H, Weber T, Rescigno T N, McCurdy C W and Belkacem A May 2013 *Physical Review A* **87**(5) 052711

[100] Rescigno T N, Lengsfield B H, McCurdy C W and Parker S D June 1992 *Physical Review A* **45**(11) 7800–7809

[101] Ram N B and Krishnakumar E 2012 *The Journal of Chemical Physics* **136**(16) 164308

[102] Papp P, Urban J, Matejčík Š, Stano M and Ingolfsson O 2006 *The Journal of Chemical Physics* **125**(20) 204301

[103] Mauracher A, Denifl S, Aleem A, Wendt N, Zappa F, Cicman P, Probst M, Märk T D, Scheier P, Flosadóttir H D, Ingólfsson O and Illenberger E 2007 *Physical Chemistry Chemical Physics* **9**(42) 5680

[104] Feyer V, Plekan O, Richter R, Coreno M, Vall-llosera G, Prince K C, Trofimov A B, Zaytseva I L, Moskovskaya T E, Gromov E V and Schirmer J May 2009 *The Journal of Physical Chemistry A* **113**(19) 5736–5742

[105] Maddern T, Francis-Staite J, Brunger M J, Jamier V, Smith S V and Buckman S J March 2009 *private communication*

[106] Ferreira da Silva F, Matias C, Almeida D, García G, Ingólfsson O, Flosadóttir H D, Ómarsson B, Ptasinska S, Puschnigg B, Scheier P, Limão-Vieira P and Denifl S November 2013 *Journal of The American Society for Mass Spectrometry* **24**(11) 1787–1797

[107] Kawarai Y, Weber T, Azuma Y, Winstead C, McKoy V, Belkacem A and Slaughter D S November 2014 *The Journal of Physical Chemistry Letters* **5**(21) 3854–3858
[108] Stapelfeldt H and Seideman T April 2003 *Reviews of Modern Physics* **75**(2) 543–557
[109] Postler J, Vizcaino V, Denifl S, Zappa F, Ralser S, Daxner M, Illenberger E and Scheier P August 2014 *The Journal of Physical Chemistry A* **118**(33) 6553–6559
[110] Streibel T and Zimmermann R June 2014 *Annual Review of Analytical Chemistry* **7**(1) 361–381
[111] Kostko O, Kim S K, Leone S R and Ahmed M December 2009 *The Journal of Physical Chemistry A* **113**(52) 14206–14211